Investigation of Electron-Distribution Function and Dynamo Mechanisms in a Reversed-Field Pinch by Analysis of Hydrogen-Pellet Deflection

L. Garzotti,[1] B. Pégourié,[2] R. Bartiromo,[1] P. Innocente,[1] and S. Martini[1]
[1]*Consorzio RFX, Corso Stati Uniti 4, 35127 Padova, Italy*
[2]*Association EURATOM-CEA sur la Fusion Contrôlée, C.E. Cadarache, 13108 Saint-Paul-lez-Durance, France*
(Received 22 October 1999)

In reversed-field pinches, two different mechanisms have been proposed to explain the dynamo process which drives the poloidal current needed to sustain the magnetic configuration: the kinetic dynamo theory and the magnetohydrodynamic (MHD) dynamo theory. Experimentally, they can be distinguished by the radial behavior of the electron distribution function. In this Letter the trajectory deflection of frozen hydrogen pellets has been used as a diagnostic of suprathermal electrons in the plasma. The classical Spitzer-Härm distortion of the electron distribution function consistent with the MHD dynamo electric field is found to give a better modeling of the pellet trajectory.

PACS numbers: 52.55.Dy, 52.65.–y, 52.70.–m

It is universally recognized that most of the matter in the universe is in the plasma state and that these plasmas are always embedded in a self-generated magnetic field. On a planetary, stellar, and galactic scale, a dynamo mechanism converts kinetic to magnetic energy and it is now clear that this is made possible by the random fluctuating component of both the velocity and magnetic field in the plasma [1].

The reversed-field pinch (RFP) is the only laboratory device which allows one to reproduce, in a broad sense, the basic mechanism of astrophysical dynamos and to document in some detail its microscopic dynamic behavior [2]. Indeed, it is experimentally well established that this toroidal magnetic configuration can be sustained by applying a toroidal electric field only. This entails a dynamo mechanism which drives the poloidal current in the region where the magnetic toroidal field component changes sign. Two different mechanisms have been proposed to explain the RFP dynamo: the kinetic dynamo theory (KDT) [3] and the magnetohydrodynamic (MHD) dynamo [4]. In the framework of the KDT the dynamo current is driven as follows: suprathermal electrons (hereafter referred to as KD electrons) are accelerated in the plasma core by the externally applied toroidal electric field and collisionless diffuse towards the plasma edge traveling along stochastic magnetic field lines. Numerical calculations have shown that the KDT could in principle account for a stationary RFP configuration [5,6] where the KD electrons would provide a substantial contribution to the poloidal current in the plasma outer region.

While the KDT relies on the magnetic field stochasticity due to the fluctuations of the confining field, the MHD dynamo mechanism is also based on magnetic fluctuations [4], but in the latter case it is their quadratic effect with coherent fluctuations of the velocity fields which generates the mean electric field necessary to drive the parallel current density everywhere in the plasma. It should be noted that, taking into account the relatively low temperature of present RFPs, such a MHD dynamo electric field is associated with a substantial classical Spitzer-Härm distortion of the electron distribution function [7]. Hence both the KDT and the MHD dynamo are consistent with the presence of suprathermal electrons in the plasma. The main difference is that the KDT predicts the suprathermal tails to be much more robust at the edge and less so in the core compared to the MHD dynamo, as highlighted also in [6].

In favor of the KDT many experiments [8–11] reported edge probe measurements of suprathermal electron tails which could account for a large fraction of the edge current density. Conversely, it was noted elsewhere [12] that the insensitivity of the magnetic profiles to plasma collisionality calls for the presence of an MHD dynamo, and a recent work [7] has shown that the edge probe measurements on the Reversed-Field Experiment (RFX) are consistent with the MHD dynamo.

A useful diagnostic tool for the suprathermal electron populations is the analysis of the ablation process of frozen hydrogen pellets injected into the plasma. As supported by experimental data [13,14] the effect of the suprathermal electrons is to enhance the pellet ablation rate and, since the tail is stronger on the electron drift side, to accelerate the pellet along the magnetic field due to the rocket effect resulting from asymmetric ablation. The sensitivity of the method is linked to the fact that the most efficient electrons for ablating the pellet are those whose energy is 5–10 times the local temperature, which is the range of energy where the distortion of the Maxwellian distribution is expected to become significant. The effect depends on the local characteristics of the electron distribution function. The pellet penetration and trajectory can be measured throughout the plasma cross section, therefore the technique provides very valuable space-resolved information.

This Letter presents a study of the trajectory deflection and the penetration of hydrogen pellets injected into a reversed-field pinch, which are found to be well accounted for by the classical Spitzer-Härm distortion of the

 0031-9007/00/84(24)/5532(4)$15.00

Maxwellian distribution function caused by the MHD dynamo electric field.

The pellets analyzed in the following were injected on RFX (minor radius $a = 0.46$ m, major radius $R = 2$ m) [15] into discharges with plasma current $I_p \approx 700$ kA, density $n_e \approx 2\text{–}4 \times 10^{19}$ m^{-3}, and temperature $T_e \approx 250$ eV. Two types of pellets are considered in particular: small pellets with particle content $N_p = 1.5 \times 10^{20}$ atoms and velocity $V_p = 400\text{–}500$ m/s, which penetrate up to the center of the discharge and exhibit a moderate deflection ($\leq$20 cm); larger pellets of 5.0×10^{20} atoms injected at 100–120 m/s, which suffer a dramatic deflection and completely ablate at the plasma periphery ($r/a \geq 0.5$). The above two cases are well representative of the typical behavior found in a larger database of 70 well documented experiments [16].

The diagnostics for the pellet ablation and trajectory is a H_α emission analyzer composed of a set of position sensitive detectors (PSD) [17] tracking the position of the barycenter of the emitting cloud and permitting a three-dimensional reconstruction of the pellet trajectory. The acquisition frequency is 50 kHz (about 70 points per trajectory), the absolute space resolution is a few millimeters, but is limited in practice to about half the size of the ablation cloud due to the nonuniformity of the H_α radiation: i.e., $\approx$1.2 cm perpendicularly to the magnetic field and $\approx$2.5 cm along the magnetic field. As said above, the deflection of the pellet trajectory results from an acceleration along the magnetic field, due to the unbalance of ablation between the electron and ion drift sides. The magnitude of this acceleration is given by the conservation of the momentum of the pellet-cloud system [18]:

$$N_p \frac{dV_p}{dt} = \frac{1}{2}\left(\frac{dN_{p,e}}{dt} - \frac{dN_{p,i}}{dt}\right)v_{\exp}. \qquad (1)$$

Here $dN_{p,e-i}/dt$ are the local ablation rates on the electron and ion side, respectively, $v_{\exp}$ is the expansion velocity of the ablated material and the factor $1/2$ accounts for the projection of $v_{\exp}$ on the field line. In addition to the pellet initial number of particles and velocity, calculating the pellet trajectory requires thus the knowledge of the ablation rates on each side of the pellet and the expansion velocity of the ablated material. The latter, $v_{\exp}$, is equal to $\sqrt{\gamma k_B T_0/m(H_2)}$, where $\gamma = 7/5$, $m(H_2)$ is the mass of molecular hydrogen, and T_0 is the temperature of the ablatant at the pellet surface (from 2×10^{-2} to 10^{-1} eV according to [19]). An averaged value $T_0 = 5 \times 10^{-2}$ eV is used in the following simulations and we have verified that, for different T_0 values within the given range, the trajectory modifications are not larger than the cloud size. This is explained by the change in the ablation rate due to the different plasma temperature and density seen by the pellet on the displaced trajectory, which tends to compensate for the change in acceleration caused by the different value of $v_{\exp}$.

In RFPs, the magnetic field is lower than in tokamaks, the diffusion of particles larger (by a factor $\approx$100) and the stronger magnetic shear favors a rapid homogenization of the ablated material in the background plasma. The ionized part of the ablation cloud is less dense than in tokamaks by almost two orders of magnitude, as measured by interferometric techniques [20], and the shielding is essentially due to the neutral part of the ablation cloud. The corresponding ablation rate obeys the neutral gas shielding (NGS) scaling law [21]. To account for the distortion of the electron distribution function, it must be properly averaged over the latter [22], yielding the following expression for the ablation rate on each side of the pellet:

$$\frac{dN_{p,e-i}}{dt} = 3.34 \times 10^{-14} 2 n_H \pi r_p^{4/3} n^{1/3} \times \left[\int_0^\infty f_{e-i}(\epsilon)\epsilon^{5.4}\, d\epsilon\right]^{1/3}, \qquad (2)$$

where r_p is the instantaneous pellet radius, n the target plasma electron density at the pellet location, n_H the solid hydrogen atomic density. $f_{e-i}(\epsilon)$ is the electron distribution function computed according to the local plasma parameters and averaged over the range of pitch angles seen, respectively, on the electron and ion side of the pellet because of their mutual shielding. All the quantities are in MKSA units except for the temperature and energy which are in eV.

To start with, we have built a simulation to study the effects expected on a pellet injected in a RFP where the MHD dynamo generates the parallel electric field necessary to sustain the configuration. To this end the electric field has been computed as $E = \eta J_\parallel$ where η is the classical Spitzer resistivity and $J_\parallel$ is the parallel current density consistent with the external magnetic measurements according to the μ and p model [23]. The form of $f_{e-i}(\epsilon)$ to be used in (2) is deduced from Spitzer and Härm [24] (hereafter referred to as SH distribution). It depends on the effective charge of ions (Z_{eff}) and on the current density, temperature, and electron density profiles. Its typical shape is illustrated in Fig. 1.

The Z_{eff} value is given by visible bremsstrahlung measurements and a profile taken from [25]. Then, assuming a constant impurity content during pellet ablation, the Z_{eff} profile is evolved taking into account the local dilution by the ablated material. The change in the average ionization state is also varied consistently with the perturbed temperature. The current density profile is assumed to remain unchanged during pellet ablation. This is justified both theoretically, because the resistive time on the scale length of the pellet path (10–50 ms) is much longer than the ablation time (1–1.5 ms), and experimentally, since the changes in the current profile as deduced from μ and p magnetic reconstruction do not exceed 5%. The temperature profile is measured by Thomson scattering and the time behavior of the core temperature by a double

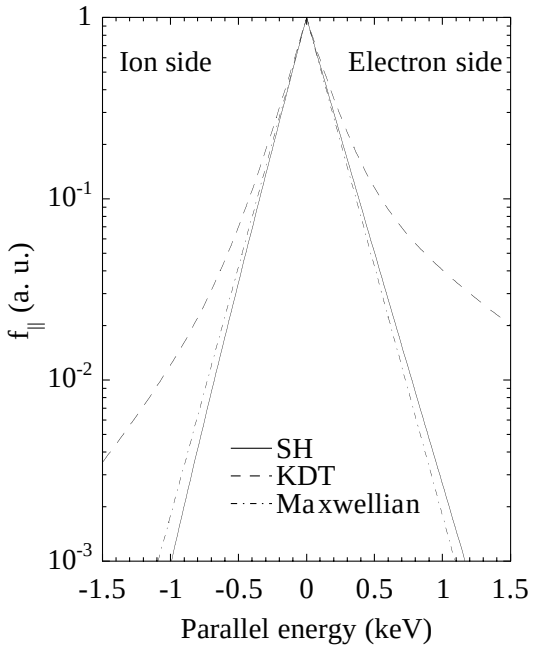

FIG. 1. The electron distribution function normalized to $f_{\parallel}(0)$ on the ion and electron side of the pellet is shown for Spitzer-Härm and KDT modeling with local plasma parameter at $r/a = 0.75$ and compared with a Maxwellian distribution.

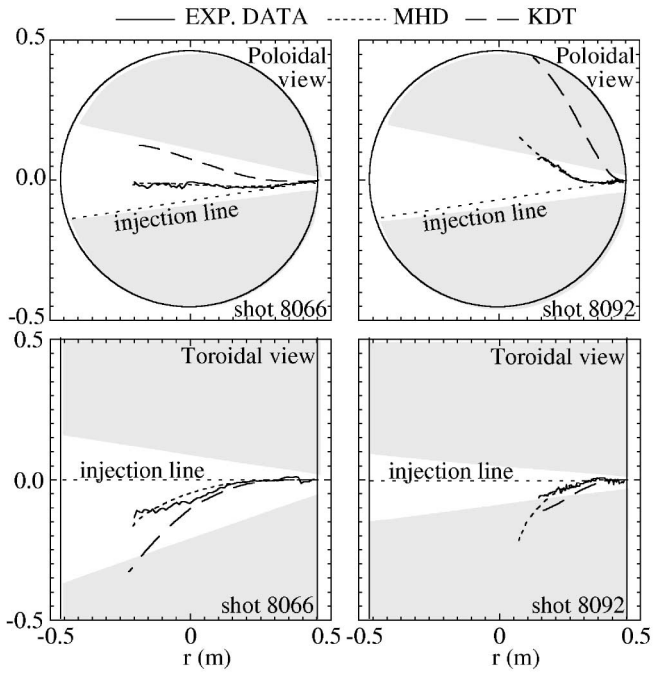

FIG. 2. Comparison of experimental and simulated pellet trajectories for the RFX shots 8066 and 8092. The shaded area is outside the H_α detector field of view. The thick line is the first wall of the device.

beryllium filter system with an acquisition frequency of 10 kHz. The electron density profile is measured by a 12-chord midinfrared interferometer with a time resolution of 4 μs. During the transient phase caused by pellet injection, the time evolution of the electron temperature has been recovered with the use of a transport simulation with empirical parameters, which fits the available experimental data.

An example of simulation of the pellet trajectory is shown on Fig. 2 for RFX shot 8066 (central penetration). In this case, which belongs to the moderate deflection dataset, a pellet with $N_p = 1.5 \times 10^{20}$ atoms is injected at $V_p = 470$ m/s from an outboard, equatorial plane, with an angle of $-7°$. The target plasma parameters are as follows: toroidal current $I_p = 670kA$, initial central density $n(0) = 3.5 \times 10^{19}$ m^{-3}, and temperature $T(0) = 250$ eV. The experimental pellet trajectory projected on the poloidal and toroidal planes are displayed in Fig. 2, together with the simulation result. On the same figure is also shown an analogous simulation for a low-velocity pellet (RFX shot 8092: injection angle $-7°$, $V_p = 123$ m/s, $N_p = 4.7 \times 10^{20}$ atoms, peripheric penetration), injected in a target plasma macroscopically similar. For both pellets, the asymmetry factor of the ablation, $A_{e-i} = [(dN_{p,e}/dt)/(dN_{p,i}/dt)]$, is between 1.1 and 1.4, with an average value of 1.2.

The agreement between simulation and experiment is satisfactory both for the pellet trajectory and penetration depth. Since the most critical parameter in the simulation is the electron temperature, we have performed a sensitivity analysis by varying its profile over the range of experimental uncertainty. In all cases the simulated pellet deflection did not change by more than twice the error of experimental data. This demonstrates that the Spitzer-Härm distortion of the electron distribution function due to the combination of the externally applied and the MHD dynamo electric fields is able to explain the pellet deflection, consistently with the experimental behavior of the plasma profiles.

In the framework of discriminating between the kinetic and the MHD dynamo theories, one should consider that the radial behavior of electron distribution function predicted by the KDT is quite different from the SH distortion consistent with the MHD dynamo. In particular, a KDT mechanism able to supply a significant fraction of the dynamo current would reduce the SH distortion in the plasma core, transforming it into a robust collisionless suprathermal tail at the plasma edge (see [6]) as illustrated in Fig. 1. This corresponds to pellet deflections and ablation rates, respectively smaller in the core and larger at the edge than predicted by SH modeling. Since the results obtained with the SH modeling are in good agreement with the experiment, one is induced to conclude that the RFX pellet data leave little room for the presence of substantial populations of KD electrons. In fact, previous results [14] obtained with a relatively small fast electron tail added to an otherwise Maxwellian plasma, which were compatible with the pellet trajectory, did not provide a substantial contribution to the parallel current density.

In order to estimate how far the predictions of KDT on pellet ablation trajectories would be from experimental data, we have done a simulation where the KD tail has been characterized according to the numerical results shown in [5,6]. Since the main differences are expected in the edge region (the difference in the core affects only high energy electrons which do not play a significant role either for the dynamo or for the ablation) we modeled the KD suprathermal tail only in the region where its contribution to the dynamo is positive (roughly for $r/a > 0.5$). The KD electrons are modeled as the sum of a Maxwellian tail with n_s equal to 10% of the local density and temperature $T_s = 2T(0)$ and of a half Maxwellian, with $n_s = 4|J_{\mathrm{dyn}}|/(e v_s)$ and temperature $T_s = 4T(0)$, where e is the electric charge and v_s the suprathermal electron velocity. The results obtained with this procedure are also displayed on Fig. 2. It can be seen that the agreement with experimental data is much worse than for the SH modeling. Indeed, in both cases, KDT simulations are well outside the error bars of the measured trajectories. This can be understood taking into account that the current density carried by the KD electrons is proportional to $n_s T_s^{1/2}$, whereas the increase of the ablation rate has a dependence $\propto n_s^{1/3} T_s^{1.64}$. It is worth noting that modeling of the KDT [5,6], which has been considered here, does not produce enough dynamo current to fully account for the experimental RFP magnetic profiles of RFX. One could therefore conclude that if such a satisfactory modeling of the dynamo could be achieved by an improved KD modeling, then it would call for even stronger disagreement with the pellet ablation data.

In conclusion, we have shown that the Spitzer-Härm distortion of the electron distribution function provides an accurate modeling of the pellet trajectories in RFX, consistent with the MHD dynamo theory. Simulations done in the presence of a fast electron population consistent with KDT modeling give much less satisfactory results. This gives confidence that in general a dynamo mechanism based on a local mean field electrodynamic theory should be able to account for the observed magnetic field. A kinetic and nonlocal approach, necessary to deal with collisionless diffusion of plasma electrons, does not provide a satisfactory description of our laboratory results.

We gratefully acknowledge the help of A. Buffa and the RFX team who made it possible to gather the experimental data on which this work is based, and E. Martines for useful discussions on the modeling of the KDT. We also want to thank in particular W. Baker, M. Fincato and the SX technical staff for their contribution to the operation of the injector.

[1] H. K. Moffat, *Magnetic Field Generation in Electrically Conducting Fluids* (Cambridge University Press, Cambridge, 1978).
[2] S. C. Prager, in *Magnetic Helicity in Space and Laboratory Plasmas*, Geophysical Monograph 111 (American Geophysical Union, Washington, DC, 1999).
[3] A. R. Jacobson and R. W. Moses, Phys. Rev. A **29**, 3335 (1984).
[4] S. Ortolani and D. D. Schnack, *The Magnetohydrodynamics of Plasma Relaxation* (World Scientific, Singapore, 1993).
[5] G. Giruzzi and E. Martines, Phys. Plasmas **1**, 2653 (1994).
[6] G. Giruzzi and S. Hokin, Plasma Phys. Controlled Fusion **38**, 1001 (1996).
[7] E. Martines, M. Shoucri, and R. Bartiromo, in *Controlled Fusion and Plasma Physics: Proceedings of the 26th European Conference, Maastricht, The Netherlands, 1999* (European Physical Society, Geneva, 1999), p. 1161.
[8] J. C. Ingraham *et al.*, Phys. Fluids **2**, 143 (1990).
[9] Y. Yagi *et al.*, Plasma Phys. Controlled Fusion **33**, 1391 (1991).
[10] V. Antoni *et al.*, Plasma Phys. Controlled Fusion **34**, 699 (1992).
[11] Y. Yagi *et al.*, Plasma Phys. Controlled Fusion **39**, 1915 (1997).
[12] T. Bolzonella *et al.*, in *Controlled Fusion and Plasma Physics: Proceedings of the 24th European Conference, Berchtesgaden, Germany, 1997* (European Physical Society, Geneva, 1997), Part I, p. 317.
[13] G. A. Wurden *et al.*, Nucl. Fusion **27**, 857 (1987).
[14] L. Garzotti *et al.*, in *Controlled Fusion and Plasma Physics: Proceedings of the 23rd European Conference, Kiev, Ukranie, 1996* (European Physical Society, Geneva, 1996), Part II, p. 637.
[15] G. Rostagni, Fusion Eng. Des. **25**, 301 (1995).
[16] F. Poli, L. Garzotti, and P. Innocente, in *Controlled Fusion and Plasma Physics: Proceedings of the 26th European Conference, Maastricht, The Netherlands, 1999* (European Physical Society, Geneva, 1999), p. 1141.
[17] P. Innocente *et al.*, Rev. Sci. Instrum. **70**, 943 (1999).
[18] V. Andersen, in *Controlled Fusion and Plasma Physics: Proceedings of the 12th European Conference, Budapest, Hungary, 1985* (European Physical Society, Geneva, 1985), Part II, p. 648.
[19] P. B. Parks *et al.*, Nucl. Fusion **17**, 539 (1977).
[20] A. Canton *et al.* (to be published).
[21] P. B. Parks and R. J. Turnbull, Phys. Fluids **21**, 1735 (1978).
[22] B. Pégourié and M. A. Dubois, Nucl. Fusion **29**, 745 (1989).
[23] V. Antoni *et al.*, Nucl. Fusion **26**, 1711 (1986).
[24] L. Jr. Spitzer and R. Härm, Phys. Rev. **89**, 977 (1953).
[25] L. Carraro *et al.*, Nucl. Fusion **36**, 1623 (1996).